Design High-Barrier and Environmentally Degradable FDCA-Based Copolyesters: Experimental and Theoretical Investigation

Han Hu, [a] Jiayi Li, [b] Ying Tian, [a] Shenggan Luo, [b] Jinggang Wang, [a] Wu Bin Ying, [a] Fenglong Li, [a] Chao Chen, [a] Yi-Lei Zhao, [b,c] Ruoyu Zhang, [a*] Jin Zhu [a*]

[a] Key Laboratory of Bio-based Polymeric Materials Technology and Application of Zhejiang Province, Ningbo Institute of Materials Technology and Engineering, Chinese Academy of Sciences, Ningbo 315201, People's Republic of China

[b] State Key Laboratory of Microbial Metabolism, Joint International Research Laboratory of Metabolic & Developmental Sciences, School of Life Sciences & Biotechnology, Shanghai Jiao Tong University, Shanghai, 200240, China.

[c] Department of Chemistry and Biochemistry, University of California, Los Angeles, California 90095, United States

Corresponding authors:

zhangruoy@nimte.ac.cn (Ruoyu Zhang);

jzhu@nimte.ac.cn (Jin Zhu)

Contents:

Total number of pages: 9

Total number of equations: 6

Total number of Figures: 3

Total number of Tables: 7

Experimental Section

Quantum Mechanical Calculations

Conformational search was performed using xTB program developed by the Grimme group.[1] During the hydrolysis reaction in PBS solution, PNDF50 and PNDF65 was built, in which the ratio of FDCA to aliphatic diacid is set at 1:1 and 2:1, respectively. During the enzymatic degradation, substrate PNDF50 was chosen for simplification. To obtain all stable configurations on the potential energy surface of the PNDF, more than 2000 possible initial geometries of PNDF were generated for conformational search using xtb software version 6.3.[1] Then these structures were optimized using semi-empirical quantum method at the PM6-DH3 level using MOPAC2016.[2] These initial geometries in a rough level conformation with relatively low energy and different geometry were screened out by Molclus.[3] The structure of each species was submitted for precise geometry optimization at M06-2X/6-31+G(d,p) level in gas phase or with SMD implicit solvation model for aqueous solution[4] using Gaussian 16 software[5], followed by frequency calculation at the same theoretical level. For conformational search of the substrate, the RMSD threshold was set for 0.5 Å, and no constraint was used.

DFT calculations of PNDF hydrolysis

Geometry optimizations were performed with B3LYP functional[6] including DFT-D3 dispersion correction[7] and 6-31G(d,p) basis set. Vibrational frequency analyses were performed at the same level of theory, to ensure local minima or first-order saddle points, and the free energies were calculated for 298.15 K and 1.0 atm. In addition, the intrinsic reaction coordinates (IRC) calculations were carried out to identify transition states and immediate reactants and products.[8]to improve the accuracy of the calculations, single-point energy calculations were performed on the optimized structures using a larger basis set 6-311+G(d,p) were performed on the optimized geometries and solvation model based on density (SMD) [4] solvation correction.

Setup of systems and Molecular dynamics Simulation

The starting crystal structure of the CALB was obtained from the protein data bank (PDB code: 1TCA). The conformation with the lowest energy was then docked into the CALB using Autodock Vina.[9] structural adjustments were made to avoid bad steric contacts. DFT optimized structure of each substrate was docked to the binding site. For the docking of the complex conformations, rigid docking was applied (i.e., no bond can rotate). We reported and used the lowest energy docking pose for further studies. The parameters of substrate PBNF were generated with the RESP[10] method and RHF/6-31* calculation[11], to generate the bonds, angles, dihedral angles and van der Waals radii

parameters for the substrate by using the Antechamber package. Following the steps above, three complex systems, PNDF-CALB were set up. Files for complexes were prepared with the *tleap* module of AMBER 18.[12] MD simulations were performed on PNDF-CALB complexes using the AMBER *ff14SB* force field.[13] The protonation states of the titratable residues (such as His, Glu, and Asp) in the complex were determined at pH consisting of experimental situation using propka.[14] Except for Asp134, which was protonated, all acidic residues were negatively charged, while Lys and Arg residues remained positively charged. The only histidine, His224 of the catalytic triad, was singly protonated at N_δ. Counterions (Na^+ and Cl^-) were added for the maintenance of system neutrality. The complexes were placed in a truncated octahedral box of water molecules, extending 12.0 Å along each dimension. Long-range electrostatic interactions were calculated with the Particle-Mesh-Ewald (PME) method, [15] and van der Waals interactions were truncated within 12 Å. The time interval was set as 2 fs, and the SHAKE[16] algorithm was used to constrain the bonds-connecting hydrogen atoms. The entire system was first minimized and heated up to 298 K before the production process. Structural analyses, such as root-mean-square deviation (RMSD), distance analysis, and clustering analysis, were conducted with the CPPTRAJ tool, implemented in Amber 18.

Non-covalent interaction (NCI) analysis

In this study, independent gradient model (IGM)[17] analysis were carried out with the Multiwfn 3.7 program[18]. Molecular plots were visualized by the VMD 1.9.3 program.[19] The IGM analysis depends on the topological characteristics of the electron density, ρ. The IGM descriptor δg^{inter} is given by the difference between the first derivatives of the charge densities for the total system and the fragments (eqs. S1):

$$\delta g(r)^{inter} = |\nabla\rho^{IGM,inter}| - |\nabla\rho| \qquad (S1)$$

$\delta g^{inter} > 0$ indicates the presence of weak interactions, and the magnitude of the descriptor at a point in space indicates the strength of the interaction.

Wavefunction analysis

The prediction of reactive sites between nucleophile and electrophile was studied by the Fukui function analysis with Hirshfeld charges.[20]The Fukui function was used to predict reactive sites at the B3LYP-D3/def-TZVP level of theory. Fukui function is defined as eqs. S2 :[21,22]

$$f(r) = \left[\frac{\partial\,\rho\,(r)}{\partial N}\right]_v \qquad (S2)$$

where N is number of electrons in present system, the constant term in the partial derivative is external potential. For a given molecular system, Fukui function was calculated using electron density of three states (eqs. S3-S5):

$$f^+(\mathrm{r}) = \rho_{N+1}(r) - \rho_N(r) \approx \rho^{LUMO}(r) \tag{S3}$$

$$f^-(r) = \rho_N(r) - \rho_{N-1}(r) \approx \rho^{HOMO}(r) \tag{S4}$$

$$f^0(r) = \frac{f^+(r) + f^-(r)}{2} = \frac{\rho_{N+1}(r) - \rho_{N-1}(r)}{2} \approx \frac{\rho^{HOMO}(r) + \rho^{LUMO}(r)}{2} \tag{S5}$$

where N is the number of electrons in the current molecular system. The $N-1$ and $N+1$ states share the same molecular geometry as the N state. For nucleophiles, f^- is the reactivity descriptor, while for electrophiles, f^+ is the descriptor. f^0 is reactivity descriptor for radical attack. Atoms with larger Fukui function tend to have higher reactivities. Isosurface maps were produced using VMD 1.9.3 program based on outputs from the Multiwfn calculations.

Molecular polarity index (MPI) was also calculated, for which is expressed as (eqs. S6):

$$\mathrm{MPI} = (1/A) \iint\limits_S |V(r)| dS \tag{S6}$$

where A and $V(r)$ refer to the area of vdW surface and value of ESP at a point r in space, respectively. The integration is performed over the whole molecular vdW surface (S). MPI is a quite reliable index of measuring molecular polarity, the larger the index, the higher the polarity.[23]
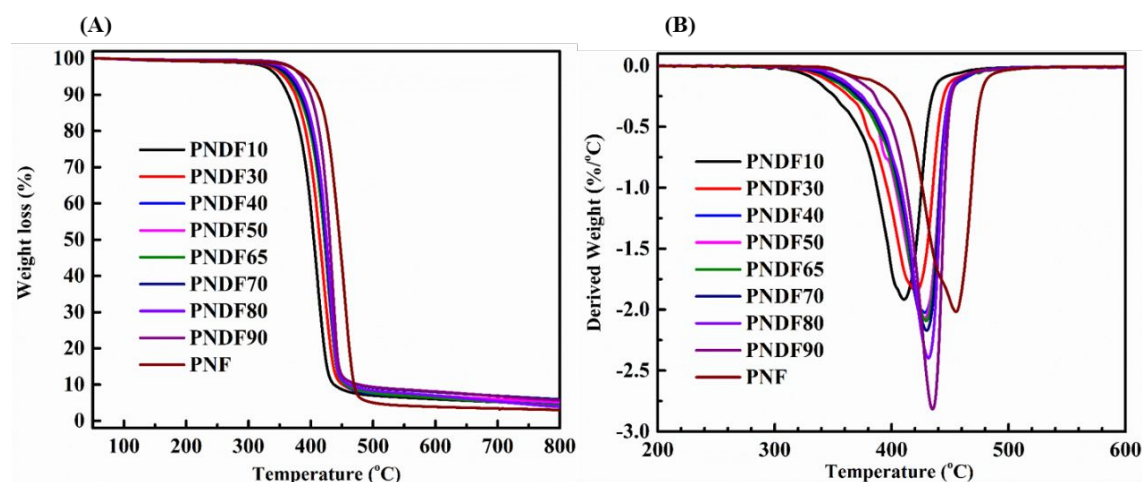

Fig. S1 (A) TGA and (B) DTG curves of PNDFs.

Table S1. Thermal properties of PNDFs.

Sample	1st heating scan		Cooling scan		2nd heating scan					TGA	
	T_m (°C)	ΔH_m (J/g)	T_c (°C)	ΔH_c (J/g)	T_g (°C)	T_{cc} (°C)	ΔH_{cc} (J/g)	T_m (°C)	ΔH_m (J/g)	$T_{5\%}$ (%)	$T_{d,max}$ (%)
PNDF10	84.1	1.6	/	/	4.0	/	/	/	/	347	410
PNDF30	54.2	0.2	/	/	16.1	/	/	/	/	357	421
PNDF40	/	/	/	/	23.5	/	/	/	/	365	428
PNDF50	/	/	/	/	28.0	/	/	/	/	369	427
PNDF65	/	/	/	/	42.2	/	/	/	/	362	430
PNDF70	/	/	/	/	45.4	/	/	/	/	365	430
PNDF80	175.4	7.2	/	/	54.7	144.9	6.8	175.0	6.8	371	431
PNDF90	191.4	27.9	/	/	64.8	144.4	27.8	190.2	27.7	385	434
PNF	202.5	29.5	/	/	70.7	146.0	32.7	200.9	32.5	391	455

Table S2. Mechanical properties of PNDFs.

Sample	E(MPa)	σ_b (MPa)	ε_b(%)
PNDF30	8±1	2.3±0.2	1400±20
PNDF40	58±2	10.4±2.6	1050±50
PNDF50	108±15	10.7±0.1	800±10
PNDF65	1665±23	45.5±6.4	340±22
PNDF70	1887±32	58.6±4.7	14±4
PNDF80	1943±28	61.5±1.5	5±1
PNDF90	2265±17	64.8±0.4	4±1
PNF	1977±28	68.1±1.5	6.0±0.6

Table S3. Recoverability of PNDF40 and PNDF50

Sample	ε (%)	$R_r(1)$ %	$R_r(2)$ %	$R_r(3)$ %	$R_r(4)$ %	$R_r(5)$ %
PNDF40	200	62.1	93.0	90.6	96.6	98.9
PNDF50	200	51.7	86.0	72.0	92.8	100.0

Table S4. Gas and water vapor permeability coefficients for PNDFs, other polymers for comparison.

Sample [a]	CO_2 (barrer) [b]	BIFp	O_2 (barrer) [c]	BIFp	H_2O (g·cm/cm^2·s·Pa) [d]	BIFp
PBAT	5.9	1	0.76	1	3.52×10^{-13}	1
PNDF40	0.043	136.8	0.050	15.3	1.43×10^{-13}	2.5
PNDF50	0.032	184.3	0.039	19.5	7.62×10^{-14}	4.6
PNDF70	0.033	178.8	0.041	18.5	4.72×10^{-14}	7.5
PNDF80	0.038	155.3	0.036	21.1	4.40×10^{-14}	8.0
PNDF90	0.035	168.6	0.033	23.0	3.68×10^{-14}	9.6

PNF	0.040	147.5	0.035	21.7	2.58×10^{-14}	13.6
PLA	1.0	5.9	0.25	3.0	1.10×10^{-13}	3.2
PEF	0.010	590	0.011	69.1	-	-
PET	0.130	45.4	0.060	12.7	-	-

[a] The test performed at low pressure (0.1001 MPa). [b] CO_2 permeability coefficient, at 23 °C, 50% relative humidity. 1 barrer = 10^{-10} cm^3·cm/cm^2·s·cmHg. [c] O_2 permeability coefficient, at 23 °C, 50% relative humidity. [d] Water vapor transmission rate, at 38 °C, 90% relative humidity.

Table S5. Molecular weight changes of PNDFs after 42 days of hydrolysis.

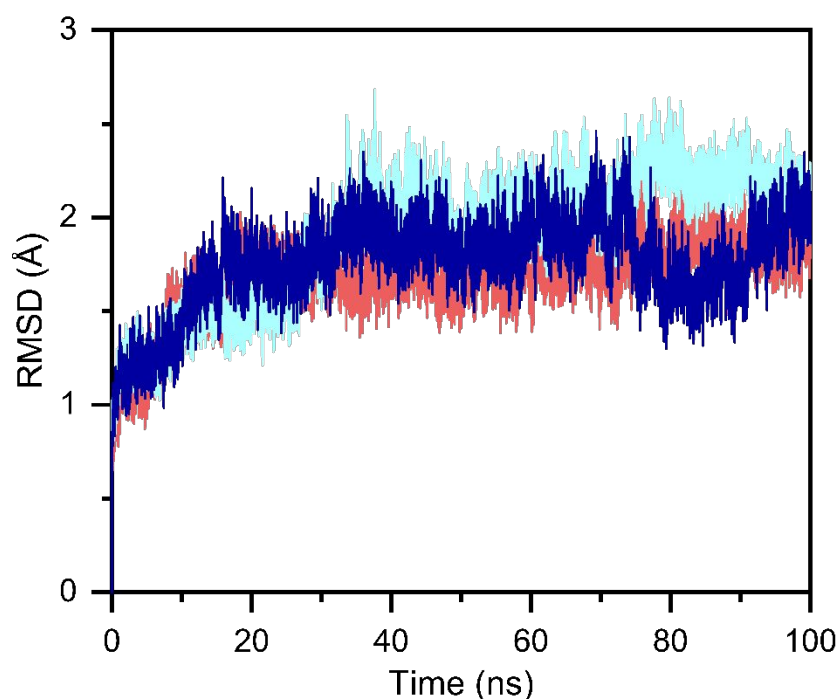| Sample	Before degradation		After 42 days of hydrolysis			
			37°C		50°C	
	M_w(g/mol)	DI	M_w(g/mol)	DI	M_w(g/mol)	DI
PNDF80	7.68×10^4	1.9	7.65×10^4	1.9	7.58×10^4	1.8
PNDF65	9.48×10^4	2.0	8.87×10^4	2.0	6.25×10^4	1.9
PNDF40	9.98×10^4	1.7	7.32×10^4	1.8	4.21×10^4	1.9
PNDF30	1.21×10^5	1.8	6.85×10^4	2.2	1.35×10^4	2.3
PNDF10	1.33×10^5	1.9	3.25×10^4	2.1	8.34×10^3	2.2

Fig. S2 Root-mean-square deviation (RMSD) of the backbone carbon atom in PNDF-CALB. The three substrate-enzyme systems were each constructed and performed three times in 100 ns molecular dynamic (MD) simulations, respectively. Stable RMSD of

the protein till the end of the simulation, suggested that the simulations were suitable for further rigorous analysis.
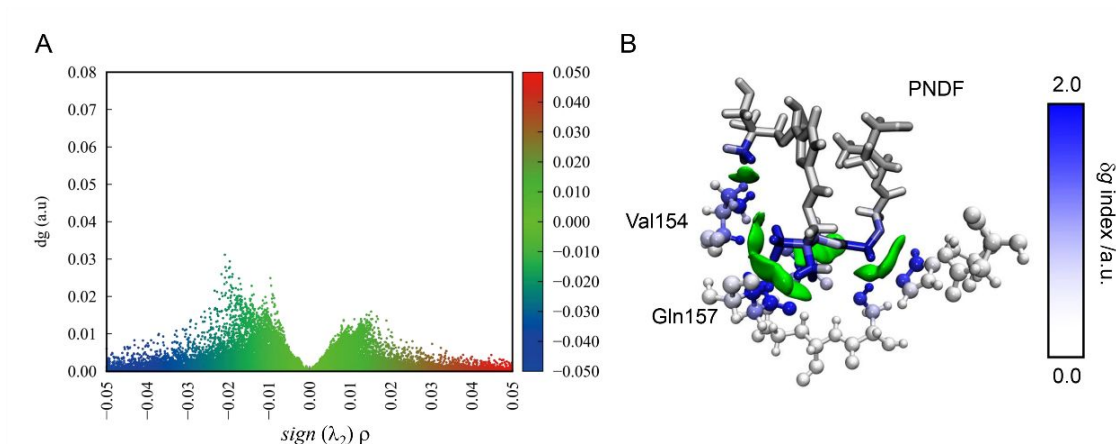

Fig. S3 Intermolecular non-covalent interaction in the PNDF-CALB. Plotting *sign* (λ_2) ρ colored IGM scatter map (A). The atoms of CALB interface colored according to their contributions to the binding with PNDF (B). White indicates no contribution to the complexation, and blue indicates the largest relative contribution

Table S6: Comparison of the values of Hirshfeld charges and Fukui functions for Carbonyl carbon atom of ester groups in PNDF50. The atom owing larger values of f^+ became the favorable sites for nucleophilic attack.

Atom	q(N)	q(N+1)	q(N-1)	f^+
C1	0.2255	0.1542	0.2308	0.0713
C2	0.2137	0.2145	0.2177	0.0007
C3	0.1896	0.1388	0.1992	0.0508
C4	0.1982	0.1626	0.2077	0.0356

Table S7: Comparison of the values of Hirshfeld charges and Fukui functions for Carbonyl carbon atom of ester groups in PNDF65. The atom owing larger values of f^+ became the favorable sites for nucleophilic attack.

Atom	q(N)	q(N+1)	q(N-1)	f^+
C1	0.2082	0.2067	0.2141	0.0015
C2	0.2100	0.2102	0.217	0.0002

C3	0.2199	0.1700	0.2223	0.0499
C4	0.2022	0.1627	0.2035	0.0395

Reference

1. Grimme, S.; Bannwarth, C.; Shushkov, P., *J. Chem. Theory Comput.* 2017, 13 (5), 1989-2009.

2. Stewart, J. J. P. MOPAC2016. Steward Computational Chemistry; http://openmopac.net/ Colorado Springs: CO, USA, 2016

3. Tian Lu, molclus program, Version 1.9.4, (accessed June 18th 2020) http://www.keinsci.com/research/molclus.html

4. Marenich, A. V., Cramer, C. J. & Truhlar, D. G, *J. Phys. Chem. B*, 2009, 113, 4538-4543.

5. Frisch, M. J.; Trucks, G. W.; Schlegel, H. B.; Scuseria, G. E.; Robb, M. A.; Cheeseman, J. R.; Scalmani, G.; Barone, V.; Petersson, G. A.; Nakatsuji, H.; Li, X.; Caricato, M.; Marenich, A. V.; Bloino, J.; Janesko, B. G.; Gomperts, R.; Mennucci, B.; Hratchian, H. P.; Ortiz, J.V.; Izmaylov, A. F.; Sonnenberg, J. L.; Williams; Ding, F.; Lipparini, F.; Egidi, F.; Goings, J.; Peng, B.; Petrone, A.; Henderson, T.; Ranasinghe, D.; Zakrzewski, V. G.; Gao, J.; Rega, N.; Zheng, G.; Liang, W.; Hada, M.; Ehara, M.; Toyota, K.; Fukuda, R.; Hasegawa, J.; Ishida, M.; Nakajima, T.; Honda, Y.; Kitao, O.; Nakai, H.; Vreven, T.; Throssell, K.; Montgomery, Jr., J. A.; Peralta, J. E.; Ogliaro, F.; Bearpark, M. J.; Heyd, J. J.; Brothers, E. N.; Kudin, K. N.; Staroverov, V. N.; Keith, T. A.; Kobayashi, R.; Normand, J.; Raghavachari, K.; Rendell, A. P.; Burant, J.C.; Iyengar, S. S.; Tomasi, J.; Cossi, M.; Millam, J. M.; Klene, M.; Adamo, C.; Cammi, R.; Ochterski, J. W.; Martin, R. L.; Morokuma, K.; Farkas, O.; Foresman, J. B.; Fox, D. J. Gaussian 16, Revision A.03; Wallingford, CT, 2016.

6. Lee, C.; Yang, W.; Parr, R. G, *Phys. Rev. B: Condens. Matter Mater. Phys*. **1988**, 37, 785.

7. Risthaus, T.; Grimme, S, *J. Chem. Theory Comput.* **2013**, 9, 1580-159

8. Maeda, S.; Harabuchi, Y.; Ono, Y.; Taketsugu, T.; Morokuma, K, *Int. J. Quantum Chem.* **2015**, *115*, 258–269.

9. O. Trott, A. J. Olson, *J.Comput. Chem* 31 (2010) 455-46

10. W. D. Cornell, P. Cieplak, C. I. Bayly, I. R. Gould, K. M. Merz, D. M. Ferguson, D. C. Spellmeyer, T. Fox, J. W. Caldwell and P. A. A. Kollman, *J. Am. Chem. Soc.*, **1995**, 117(19), 5179-5197

11. H. Stoll, G. Wagenblast and H. Preuss, *J. Am. Chem. Soc.*, **1978**, 100(24), 7742–7743.

12. Case DA, Ben-Shalom IY, Brozell SR, Cerutti DS, Cheatham TE, Cruzeiro VWD (2018) AMBER18, University of California, San Francisco.

13. J. A. Maier, C. Martinez, K. Kasavajhala, L. Wickstrom and K. E. Hauser, Simmerling, C, *J. Chem. Theory Comput.,* **2015**, 11(8), 3696-3713.

14. T. J. Dolinsky, J. E. Nielsen, J. A. McCammon and N. A. Baker, *Nucleic Acids Res.*, **2004**, 32(W), W665-W667

15. T. Darden, D. York and L. Pedersen, *J. Chem. Phys.*, **1993**, 98(12), 10089–10092.

16. J. P. Ryckaert, G. Ciccotti and H. J. C. Berendsen, *J. Chem. Phys.,* **1977**, 23(3), 327-341.

17. Lefebvre, C., Rubez, G., Khartabil, H., Boisson, J. C., Contreras-García, J., and Hénon, E, *Phys. Chem. Chem. Phys.* 2017, 19, 17928-17936.

18. Lu, T.; Chen, F., *J. Comput. Chem*. **2012**, 33 (5), 580-592.

19. Humphrey, W.; Dalke, A.; Schulten, K., *J. Mol. Graphics* **1996**, 14 (1), 33-38.

20. Wang Y, Zhang C, Zhao YL, Zhao R, Houk KN. Biomolecules. **2020**, 10(6), 815.

21. Parr, R. G.; Yang, W, *J. Am. Chem. Soc.* 1984, 106, 4049-4050.

22. Fukui, K.; Yonezawa, T.; Shingu, H, *J. Chem. Phys*. 1952, 20, 722-725

23. Liu, Z., Lu, T., & Chen, Q. *Carbon,*2021,171, 514–523.